Title: CD301b lectin expression in the breast tumor microenvironment augments tumor growth

Authors: Ahmet Ozdilek[1]†, Amy V. Paschall[1]†, Zahra Nawaz[1], Afaq M. M. Niyas[1], and Fikri Y. Avci[1*]

Affiliations: [1]Department of Biochemistry, Emory Vaccine Center, Winship Cancer Institute, Emory University School of Medicine, Atlanta, GA 30322

†**These authors contributed equally.**

*Corresponding author. Email: favci@emory.edu

Abstract

Aberrant tumor glycosylation can alter immune recognition; however, the specific influence of glycan-lectin interactions on tumor progression remains poorly understood. Here, we identify the C-type lectin receptor CD301b (encoded by *Mgl2*) as a regulator of immune activity within the breast tumor microenvironment (TME). Using a murine triple-negative breast cancer model, we demonstrate that tumors expressing the Tn glycoantigen grow more rapidly, and this growth is facilitated by CD301b$^+$ immune cells. Depletion or genetic loss of CD301b markedly suppressed tumor growth, indicating that CD301b promotes tumor progression through myeloid-tumor interactions. Phenotypic analyses revealed that CD301b$^+$ cells within tumors are type 2 conventional dendritic cells (cDC2s), a subset known to influence immune polarization. Single-cell RNA sequencing of human breast cancers showed that the human ortholog CLEC10A is expressed in cDC2-like dendritic cells and select macrophage subsets, suggesting a conserved role for CD301$^+$ myeloid populations. Transcriptomic profiling of tumors developed in *Mgl2*-deficient mice revealed a shift toward an inflammatory, immune-activated state consistent with enhanced antitumor immunity. Together, these findings establish a link between tumor glycosylation and lectin signaling of myeloid cells, highlighting CD301b as a potential target for reprogramming the tumor immune microenvironment in breast cancer.

Introduction

A major setback observed in many cancers arises from immune modulation within the tumor microenvironment (TME), preventing effective anti-cancer responses. Vaccines, CAR T cells, and checkpoint blockade prime the immune system against cancer-associated antigens, promoting cancer cell destruction through immune cytotoxicity [1]. Immune therapies for breast cancer remain largely ineffective due to the ability of the tumor to grow unimpeded and eventually metastasize. Immune regulation can occur through cytokine secretion (such as IL-10), signaling mechanisms, or checkpoints (such as through PD-1) [2-5]. During the malignant transformation of a mammalian cell, a dramatic and aberrant modification of cellular glycosylation is observed. Tumor-associated carbohydrate antigens, or TACAs, can induce immune suppression, allowing cancer cells to evade immune cells [6-8]. Lectins are carbohydrate-binding proteins that function as receptors for immune cells and can activate immune regulatory pathways through their interactions with TACAs [9-11]. Similarly, modulating immune profiles in the TME by engaging sialic-acid-binding immunoglobulin-like lectins (Siglecs) is a known TACA mechanism [12-14]. Thus, elucidating the roles of lectins in regulating the immune response within the TME is becoming increasingly important.

Tn antigen is a TACA ranked as a high-priority cancer-associated antigen based on its antigenicity and oncogenicity [11,15-19]. Tn is a truncated form of the cell surface O-glycan, consisting of the terminal O-linked N-acetylgalactosamine (GalNAc) attached to serine or threonine. The aberrant glycosylation associated with Tn may occur when the enzyme responsible for O-glycan elongation, T-synthase or its associated chaperone, Cosmc (C1GALT1C1), becomes functionally inhibited [20,21]. Tn-expressing mucin 1 (MUC1) has been associated with breast cancer cells [22,23], especially in triple-negative breast cancer [24,25]. Modulating MUC1 expression or Tn glycosylation can inhibit tumor growth [26-28]. However, developing immune responses against Tn-MUC1 has been problematic [29].

52 CD301, also known as macrophage galactose-type lectin (MGL) or CLEC10A, is a C-type lectin
53 receptor (CLR) that binds to Tn antigen on the surface proteins in humans [19,30]. In mice, the Tn-
54 recognizing homolog of the human CD301 is CD301b, also known as MGL2 [19,31]. CD301b is
55 primarily expressed by myeloid cells such as dendritic cells (DCs) and macrophages [17]. Previously,
56 CD301b-expressing myeloid cell populations have been linked with immunosuppressive responses
57 [16,17,19,32-34]. DCs and macrophages can suppress the proliferation of $CD4^+$ effector T lymphocytes
58 through the interaction of MGL with terminal GalNAc residues on CD45 expressed by T cells [17].
59 This cell-specific glycosylation of CD45 provided an immunoregulatory pathway, mediated by
60 MGL, thereby controlling effector T cell function. In another study, $CD301b^+$ dendritic cells
61 suppressed T follicular helper cells and antibody responses to protein antigens [32]. Recently, an
62 immunosuppressive DC subset expressing CD301b was shown to accumulate at secondary sites
63 and promote metastasis in pancreatic cancer [34] and lung cancer [35].
64 In this study, we investigated the role of CD301b in a murine model of triple-negative breast cancer
65 and found that the loss of CD301b expression significantly restricted tumor growth. Within the
66 tumor microenvironment, CD301b-expressing immune cells were identified as type 2 conventional
67 dendritic cells. Analysis of publicly available single-cell RNA sequencing (scRNA-seq) datasets
68 revealed similar CD301-expressing myeloid cell populations in human breast cancer tissues,
69 suggesting that this regulatory axis may extend beyond the murine model. To further explore the
70 mechanisms underlying the observed tumor growth restriction, we performed bulk RNA
71 sequencing (bulk RNA-seq) on murine tumors, which showed heightened inflammatory immune
72 responses when CD301b was absent. Together, these findings link CD301 expression to the control
73 of tumor-associated inflammation and point to its potential as a target for new breast cancer
74 therapies.

75 **Results**

76

77 ***CD301b/Tn Axis Impacts Tumor Growth.***

78 We first aimed to investigate the relationship between CD301b^{+} immune cells and Tn glycoantigen-
79 expressing breast cancer cells. We used a CRISPR-Cas9 gene editing model to knock out Cosmc
80 expression in AT3 murine breast cancer cells. Cosmc is a chaperone essential in elongating the core
81 O-glycan beyond the truncated Tn form of α-GalNAc [20,21,36]. When the Cosmc function/expression
82 is disrupted, elongation of the O-glycan is not observed; instead, the Tn antigen is observed at
83 significantly higher levels. After disrupting Cosmc expression in these cell lines, we confirmed
84 increased Tn cell surface expression through flow cytometry using both a reBaGs6 IgM antibody
85 (Suppl. Fig. 1A) [37] as well as a complementary biotinylated VVL lectin coupled with fluorescent
86 streptavidin (Suppl. Fig. 1B). Both staining methods indicated significantly higher Tn expression
87 on the *Cosmc* KO cell line. We also isolated RNA from each cell line and confirmed decreased
88 Cosmc expression in the Tn^{hi} cell line through qPCR using *Cosmc* primers (Suppl. Fig. 1C). We
89 then tested whether knocking out Cosmc expression changes the proliferation rate of the AT3 breast
90 cancer cells *in vitro*. After culturing both cell lines at the same concentrations for three days, we
91 observed no significant differences in cell proliferation between the two lines (Suppl. Fig. 1D),
92 indicating that Tn expression alone does not promote cancer cell growth.
93 To determine *in vivo* tumor cell growth, we injected AT3 (Tn^{lo}) and AT3 *Cosmc* KO (Tn^{hi}) murine
94 breast tumor cells into the mammary pads of C57BL/6 mice and monitored tumor growth. We
95 observed that Tn^{hi} tumors grew significantly faster than Tn^{lo} tumors (Fig. 1A), indicating that Tn
96 expression impacts tumor growth rate.
97 To examine the contribution of CD301b-expressing immune cells to tumor growth, we employed
98 heterozygous *Mgl2$^{+/DTReGFP}$* mice (Mgl2-DTR), in which CD301b+ immune cells can be selectively
99 depleted by diphtheria toxin (DT) treatment [32,33]. In the first experiment (Fig. 1B), AT3 Tn^{low} or
100 Tn^{hi} tumor cells were injected into Mgl2-DTR mice with or without DT administration. Tumor
101 growth was significantly reduced in DT-treated mice of the Tn^{hi} group, indicating that CD301b^{+}
102 immune cells promote tumor progression. In a complementary experiment (Fig. 1C), we injected

103 AT3 Tn^{hi} cells into homozygous *Mgl2*$^{DTReGFP/DTReGFP}$ mice (CD301b-null, *Mgl2* KO), which lack
104 surface expression of CD301b due to the disruption of both alleles but retain the immune cell
105 populations. These mice also exhibited markedly reduced tumor growth compared with wild-type
106 controls. Together, these experiments indicate that the observed phenotype is associated with tumor
107 Tn expression and facilitated by the CD301b protein.

108 ***Tumor-infiltrating CD301b^{+} cells display a type 2 conventional dendritic cell (cDC2) phenotype.***

109 We next characterized tumor-infiltrating CD45^{+}CD301b^{+} immune cells in the murine triple-
110 negative breast cancer model. These cells expressed CD11c, a canonical dendritic cell (DC)
111 marker [38,39] (Fig. 2A) and were strongly positive for MHCII, confirming their DC identity (Fig.
112 2B). CD301b^{+} cells also expressed CD11b, a defining marker of mouse type 2 conventional
113 dendritic cells (cDC2s) [40] (Fig. 2B). Mouse cDC2s can be distinguished from cDC1s by CD103
114 and SIRP-alpha expressions [38,41]. We examined the expression of these markers by tumor-
115 infiltrating CD301b^{+} cells, which display a cDC2s phenotype (Fig. 2C). Although CD301b^{+} cells
116 are primarily cDC2s, not all DCs or cDC2s express CD301b in the TME (Fig. 2D and 2E).

117 cDC2s constitute a subset of antigen-presenting cells that play key roles in coordinating adaptive
118 immune responses. In contrast to cDC1s, which specialize in cross-presentation and cytotoxic T
119 cell activation, cDC2s promote CD4^{+} T cell priming and modulate immune polarization within
120 tissues [42-44]. Recent studies have shown that cDC2s exhibit remarkable plasticity in the tumor
121 microenvironment, where they can adopt either immunostimulatory or tolerogenic phenotypes in
122 response to local cues [44].

123 ***CD301^{+} immune cells in the human breast cancer TME include both dendritic cells and***
124 ***macrophages***

125 Since CD301b^{+} cells in the murine tumor microenvironment were identified as cDC2s, we then
126 investigated whether CD301 expression in human breast cancers similarly correlated with dendritic
127 cells or extended to other myeloid subsets. To address this, we analyzed publicly available single-

128 cell RNA sequencing (scRNA-seq) data (GSE161529) from 20 patients, including triple-negative
129 (n = 8), ER$^+$ (n = 6), and HER2$^+$ (n = 6) tumors [45]. Following quality control, data integration and
130 annotation, we focused on CD45$^+$ immune cells to map CLEC10A (human CD301) expression
131 across myeloid populations (Fig. 3A; Suppl. Fig. 3A). CLEC10A expression was most prominent
132 in dendritic cells and was also detectable in macrophage/monocyte populations, with negligible
133 expression in other immune cells (Fig. 3B–C). Across breast cancer subtypes, dendritic cells
134 consistently showed higher CLEC10A expression than macrophages (Suppl. Fig. 3B). Within the
135 dendritic cell compartment, we identified four subsets—cDC1, cDC2, cDC-LAMP3$^+$, and
136 plasmacytoid DC (pDC)—and found that CLEC10A expression was highest in cDC2 (56.9%) and
137 moderate in cDC-LAMP3$^+$ (11.3%), but low in cDC1 (1.9%) and absent in pDCs (0%) (Fig. 3D–
138 F; Suppl. Fig. 3C–D).
139 We next examined tumor-associated macrophages (TAMs). TAMs are key regulators of tumor
140 inflammation, tissue remodeling, and immune suppression [46]. TAMs were subdivided into
141 transcriptionally defined subsets reflecting distinct functional programs: C1QC$^+$ macrophages,
142 associated with immunosuppression [47-49]; NLRP3$^+$ macrophages, associated with poor prognosis
143 and tumor growth [50,51]; and INHBA$^+$ macrophages, linked to angiogenesis, matrix remodeling, and
144 tumor progression [52] (Fig. 3G; Suppl. Fig. 3E). Among these subsets, *CLEC10A* transcription
145 distributed similarly in C1QC$^+$ macrophages (11%), NLRP3$^+$ macrophages (9%), and INHBA$^+$
146 macrophages (7%) (Fig. 3H–I). Interestingly, CLEC10A-positive NLRP3$^+$ macrophages were
147 detected exclusively in triple-negative breast cancers, where expression levels were comparable to
148 those in INHBA$^+$ macrophages (Suppl. Fig. 3F). This enrichment suggests that CD301 expression
149 extends beyond dendritic cells to select macrophage populations, particularly those engaged in
150 inflammatory and tissue-remodeling responses within aggressive tumor subtypes.
151 Taken together, these results indicate that CD301 expression in the human breast cancer
152 microenvironment is concentrated within myeloid lineages—encompassing both cDC2-like

153 dendritic cells and specialized macrophage subsets. This pattern mirrors the cellular distribution
154 observed in the mouse TME, suggesting that CD301 marks a conserved myeloid program
155 potentially involved in coordinating immune regulation and tissue remodeling during tumor
156 progression.

157 ***The lack of CD301b is associated with a strong inflammatory immune signature in the breast***
158 ***TME***

159 Since CD301b directly associates with tumor growth and identifies cDC2 and macrophage
160 populations within the breast tumor microenvironment (TME), we then examined how its loss
161 impacts immune signaling and tumor–immune interactions. To this end, we performed bulk RNA
162 sequencing (bulk RNA-seq) on tumors derived from wild-type (WT) and *Mgl2* knockout (*Mgl2*
163 KO) mice following injection of AT3 Tn^{hi} tumor cells. The global transcriptomic heatmap (Fig.
164 4A) revealed distinct clustering and clear separation between WT and *Mgl2* KO mouse tumors,
165 indicating a strong transcriptional divergence associated with *Mgl2* loss. This observation provided
166 the foundation for downstream pathway and gene-level analyses to elucidate how CD301b
167 influences immune regulation within the TME.

168 To dissect these transcriptomic differences, Gene Set Enrichment Analysis (GSEA) was performed
169 using the Hallmark and Kyoto Encyclopedia of Genes and Genomes (KEGG) enrichment gene set
170 databases (Fig. 4B–C). *Mgl2* KO tumors displayed significant enrichment of immune and
171 inflammatory pathways, including TNF-α/NF-κB, IL-6/JAK-STAT3, interferon-α/γ, and IL-17
172 signaling—pathways broadly associated with myeloid activation, cytokine production, and tumor
173 immunosurveillance [53,54]. Despite the slower tumor growth observed in the knockout mice,
174 complement/coagulation, hypoxia, and glycolytic pathways were also upregulated, suggesting a
175 compensatory increase in metabolic and inflammatory activity within the TME. Collectively, these
176 data indicate that CD301b functions as an immunoregulatory node that tempers cytokine and
177 interferon responses, whereas its loss enhances pro-inflammatory signaling. The dominance of

178 interferon- and NF-κB–driven programs aligns with the slower tumor progression observed in KO
179 mice, implying that CD301b deficiency reprograms the TME toward a functionally immune-active,
180 tumor-controlling state.

181 The pathway-focused volcano plot (Fig. 4D) highlights key upregulated genes underpinning these
182 responses, including *Cxcl3, Il1a, Il23a, Il36g, Csf3, Nos2, S100a8, S100a9,* and *Lcn2*. These
183 represent canonical NF-κB and IL-17 targets known to mediate myeloid recruitment, nitric oxide
184 production, and acute-phase inflammation—hallmarks of innate immune activation [55-57]. The
185 upregulation of the serine protease inhibitor and matrix metalloproteinase genes *Serpinb2* and
186 *Mmp10* in the tumor microenvironment of knockout mice suggests a tumor-suppressive function
187 through the regulation of extracellular matrix remodeling and modulation of immune responses
188 [58,59]. Thus, CD301b loss produces a highly activated, cytokine-rich TME that maintains elements
189 of tissue repair while fostering effector cell response and immune surveillance.

190 The volcano plot of all differentially expressed genes (DEGs) (Fig. 4E) contextualizes these
191 changes within the full transcriptome. Upregulated genes largely mirrored those driving enriched
192 pathways, confirming that *Cxcl3, Il1a, Il23a, Nos2, S100a8/a9,* and *Csf3* constitute the core *Mgl2*
193 KO transcriptional program rather than isolated pathway artifacts. On the other hand,
194 downregulation of the TGF-β family growth differentiation factor 3 and the apelin receptor genes
195 *Gdf3* and *Aplnr* is associated with promoting tumor growth, angiogenesis, and metastasis [60,61].

196 Together, these results suggest that CD301b deficiency reprograms the TME toward a cytokine-
197 driven, inflammatory, and interferon-dominant state that enhances immune activation and tumor
198 control. The loss of CD301b lifts an immunoregulatory brake within the TME, unleashing broad
199 inflammatory signaling that, despite introducing metabolic stress, creates a net anti-tumor
200 environment characterized by immune activation and delayed tumor growth.

201 **Discussion**

202 Aberrant glycosylation is a defining hallmark of malignant transformation, and our findings identify
203 CD301b as a key immunoregulatory lectin linking breast tumor-associated Tn antigens to myeloid
204 immune modulation. CD301b^{+} cells, primarily cDC2s, promoted breast tumor growth, whereas
205 their depletion or genetic loss limited progression. These observations align with previous studies
206 demonstrating that TACAs interact with lectins to influence myeloid differentiation and immune
207 regulation [19,21,22,62-64].
208 Transcriptomic profiling of tumors developed in *Mgl2*-deficient mice revealed broad activation of
209 NF-κB, IL-6–JAK–STAT3, and interferon pathways, consistent with a shift toward a pro-
210 inflammatory, "immune-hot" microenvironment [65]. These data position CD301b as an
211 immunoregulatory node that tempers innate activation, similar in concept to a checkpoint-like
212 mechanism operating within the myeloid compartment [9,10,66,67]. While this study does not define
213 the signaling circuitry involved, it indicates that CD301b expression in cDC2s and macrophages
214 contributes to a previously unrecognized immunoregulatory phenotype in breast cancer TME.
215 The complex and pleiotropic nature of CD301b's activity may explain its influence on the immune
216 landscape of cancer [66-68]. CD301b's modulatory behavior mirrors that of other C-type lectin
217 receptors [69]. CD301b-mediated restraint may protect against chronic inflammation, but in tumors,
218 it can inadvertently favor immune escape [70,71]. Conversely, CD301b loss triggers inflammation
219 driven by NF-κB and interferons, which enhances effector recruitment but imposes metabolic and
220 hypoxic stress on the TME [72]. Together, these findings support a model in which CD301b functions
221 as a molecular regulator balancing immune activation and tolerance in breast cancer.
222 Mechanistically, CD301b–Tn interactions may regulate antigen processing, cytokine release, or
223 costimulatory signaling within dendritic cells, thereby shaping T cell activation thresholds [69]. These
224 possibilities remain speculative but highlight the potential of CD301b as a new immune-regulatory
225 axis distinct from canonical checkpoints, such as PD-1 or CTLA-4. Future work should investigate
226 how TACA ligands and intracellular adaptors regulate CD301b signaling and consequent immune

227 programming in the TME. Further single-cell and spatial analyses of breast TME transcriptome in
228 the presence and absence of CD301b will help define how CD301b^{+} subsets integrate into existing
229 immune networks across tumor stages.
230 From a translational perspective, targeting the CD301–Tn interaction offers a promising route to
231 remodel the breast cancer immune microenvironment. Pharmacologic blockade or glycomimetic
232 interference could complement checkpoint inhibitors by dismantling glycan-mediated myeloid
233 suppression, whereas selective induction of this pathway may have therapeutic relevance in
234 autoimmune disease [73]. Ultimately, elucidating the intricate mechanisms that govern immune
235 modulation through CD301b will be essential to selectively induce these properties in disease-
236 specific contexts, enabling the development of knowledge-based, precision immunotherapies.
237 In summary, this study identifies an immunomodulatory CD301b^{+} myeloid phenotype that
238 contributes to breast cancer growth and whose loss induces a robust inflammatory program in the
239 breast TME. While the molecular mechanisms remain to be defined, our data indicate that CD301b
240 acts as a glycan-sensitive, checkpoint-like regulator of myeloid activity. Elucidating its ligand
241 specificity and downstream signaling will clarify how breast tumor glycosylation reshapes TME
242 and may reveal new strategies to enhance immunotherapy efficacy.

243 **Materials and Methods**

244 ***Mice***

245 Eight-week-old female C57BL/6 mice were obtained from Jackson Laboratories (Bar Harbor, ME)
246 and housed at Emory University Whitehead Biomedical Research Building. *Mgl2*$^{DTReGFP/DTReGFP}$
247 mice were a generous gift from Akiko Iwasaki at Yale University. To obtain heterozygous
248 *Mgl2*$^{+/DTReGFP}$ mice, C57BL/6 were bred with *Mgl2*$^{DTReGFP/DTReGFP}$ mice. Mice were kept in
249 microisolator cages and handled under biosafety level 2 (BSL2) hoods. For tissue processing and
250 subsequent flow cytometry, mice were euthanized by carbon dioxide inhalation in accordance with
251 IACUC guidelines. Where applicable, cell suspensions were generated through mechanical tissue

252 disruption and collagenase D digestion. Red blood cells were lysed, and samples were filtered
253 through 60 μm nylon filters to obtain single-cell suspensions. For depletion of CD301b^{+} cells,
254 heterozygous Mgl2-DTR mice were treated with diphtheria toxin (0.5μg/mouse) in sterile PBS
255 intraperitoneally every two to three days, starting at day -1 before tumor injection.
256 All mouse experiments were in compliance with the Emory University Institutional Animal Care
257 and Use Committee under an approved animal use protocol. Our animal use protocol adheres to the
258 principles outlined in *U.S. Government Principles for the Utilization and Care of Vertebrate*
259 *Animals Used in Testing*, *Research and Training*, the Animal Welfare Act, the *Guide for the Care*
260 *and Use of Laboratory Animals*, and the *AVMA Guidelines for the Euthanasia of Animals*.
261 ***Generation of Tn^{hi} breast cancer cells***
262 To express Tn glycans at high levels in tumor cells, we used a CRISPR/Cas9 methodology to stably
263 silence Cosmc expression in AT3 cells using established protocols and reagents. Mouse *Cosmc*
264 guide RNA and CRISPR/Cas9 plasmid were obtained from Santa Cruz Technology (sc-425587).
265 AT3 murine breast cancer cells were a generous gift from the Kebin Liu lab at Augusta University.
266 AT3 cells were transfected with *Cosmc* CRISPR/Cas9 KO plasmid according to the manufacturer's
267 protocol. Puromycin was used to select transfected cells. We then used flow cytometry to confirm
268 higher expression of Tn on the AT3 cell surfaces using the ReBaG6 antibody (generously provided
269 by Richard Cummings at Harvard University) (Suppl. Fig. 1A) [37] and VVL lectin (Vector
270 Laboratories) (Suppl. Fig. 1B). The proliferations of transfected and untransfected cell lines (AT3
271 Tn^{hi} and AT3 Tn^{low}) were tested in an MTT proliferation assay for three days, and colorimetric
272 analysis was performed with a CytoTek plate reader according to protocol; no significant
273 differences in proliferation compared to parent cells were observed (Suppl. Fig. 1D). Cell lines were
274 maintained in RPMI media supplemented with 10% FBS, sodium pyruvate, HEPES buffer, NEAA,
275 β-mercaptoethanol, and penicillin/streptomycin at 37°C, 5% CO2.
276 ***AT3 Tn^{low} and/or AT3 Tn^{hi} Tumor Challenge***

277 AT3 cells were harvested and washed in sterile PBS. Cells were suspended in a final concentration
278 of 2.5E6/ml sterile PBS. Cells were subcutaneously injected into the mammary pads of mice at
279 2.5E5/100µl/mouse. Mice were observed and euthanized at the tumor endpoint (maximum tumor
280 dimension between 0.9 cm and 1.2 cm. Tumor volumes were calculated as ((length x width x
281 width)/2) in mm^3.

282 ***Flow Cytometry***

283 Cells were stained in PBS with TruStain fcX (BioLegend, Cat. No. 101320) to reduce non-specific
284 antibody binding. Cell samples were stained with the following antibodies and stains: CD11c-
285 PacBlue (BioLegend, clone N418), CD11b-Alexa Fluor 488 (BioLegend, clone M1/70), SIRPα-
286 Alexa Fluor 700 (BioLegend, clone P84), CD103-PE/Dazzle 594 (BioLegend, clone 2E7), MHCII-
287 BV785 (BioLegend, clone M5/114.15.2), CD45 Alexa Fluor 647 (BioLegend, clone 30-F11),
288 CD301b-PE (BioLegend, clone URA-1), and LIVE/DEAD Fixable Blue (Invitrogen). All isotype
289 controls were obtained from BioLegend. Samples were washed and analyzed with flow cytometry
290 (Cytek Aurora). Fluorescence minus one (FMO) plus specific isotype control antibody-stained
291 samples were used as negative staining controls, and single stains were used for compensation.
292 Flow cytometry data were analyzed using FlowJo Single Cell Analysis Software with gating
293 strategies shown in Suppl. Fig. 2.

294 ***Bulk RNA-seq and Bioinformatics***

295 Tumors were harvested from wild-type C57BL/6J and *Mgl2* KO mice (n = 3 per group). Total RNA
296 was extracted using the MagMAX™ mirVana™ Total RNA Isolation Kit in combination with the
297 KingFisher Apex system (Thermo Fisher Scientific). RNA integrity and concentration were
298 assessed with a Qubit 3.0 fluorometer (Thermo Fisher Scientific). High-quality RNA samples were
299 used for library preparation, followed by quality control and sequencing using Novogene's standard
300 protocol. Libraries were sequenced on the Illumina NovaSeq X Plus platform to generate paired-
301 end 150 bp reads (PE150) at Novogene Inc. Raw FASTQ files were retrieved and subjected to

302 quality control with FastQC [74]. Reads were aligned to the *Mus musculus* reference genome
303 (GRCm39/mm39) using HISAT2 [75]. A gene-level count matrix was generated with featureCounts
304 [76]. The count matrix was imported to the downstream differential expression analysis using the
305 *DESeq2* R package [77]. Significantly differentially expressed genes were defined by adjusted p-
306 value < 0.05. Gene Set Enrichment Analysis (GSEA) was performed on the RNA-seq dataset using
307 the clusterProfiler R package [78] to identify significantly enriched KEGG and hallmark pathways
308 between *Mgl2* KO and wild-type tumors. To focus on cancer-relevant biology, enrichment results
309 were refined to include immune- and cancer-related pathways.
310

311 ***Analyzing the scRNA-seq data***

312 The scRNA-seq data generated using the 10x Genomics Chromium platform from human breast
313 cancer tumors (GSE161529) [45] were obtained from Gene Expression Omnibus (GEO) [79]. Data were
314 processed into the Seurat R package (version 5), and low-quality cells were removed based on
315 established Seurat quality control parameters [80]. After QC, putative doublets were removed using
316 the *DoubletFinder* R package [81]. Datasets were integrated, and non-immune cells were removed by
317 subsetting the $CD45^+$ cells with detectable *PTPRC* expression (*PTPRC* > 0). Following
318 preprocessing, cell annotation was contacted with scATOMIC [82]. The subclasses of the dendritic
319 cells and macrophages were further validated with canonical lineage markers [83,84].

320 **Statistical Analysis**

321 GraphPad Prism v8 was used for statistical analyses. Two-way ANOVA with Tukey's multiple
322 comparisons test was used to determine statistical significance between experimental groups in
323 each of the applicable experimental models (Fig. 1B). An unpaired parametric two-tailed t-test was
324 used for Fig. 1A, 1C, 2A, 2B, 2C, 2D, 2E, and Suppl. Fig. 1C. Significance is indicated on each
325 graph based on p-value: >0.05 = ns; <.05 = *; <0.01 = **; <0.001 = ***; <0.0001 = ****.
326

Acknowledgements

We acknowledge the following individuals for their contributions of transgenic mice, cell lines, and monoclonal antibodies: Dr. Akiko Iwasaki, Dr. Kebin Liu, and Dr. Richard Cummings. National Institutes of Health grants R01AI123383 and R01AI152766 supported this work.

References

1 Zhang, Y. & Zhang, Z. The history and advances in cancer immunotherapy: understanding the characteristics of tumor-infiltrating immune cells and their therapeutic implications. *Cell Mol Immunol* **17**, 807-821 (2020). https://doi.org:10.1038/s41423-020-0488-6

2 Swoboda, A. & Nanda, R. Immune Checkpoint Blockade for Breast Cancer. *Cancer Treat Res* **173**, 155-165 (2018). https://doi.org:10.1007/978-3-319-70197-4_10

3 Fiorentino, D. F., Bond, M. W. & Mosmann, T. R. Two types of mouse T helper cell. IV. Th2 clones secrete a factor that inhibits cytokine production by Th1 clones. *J Exp Med* **170**, 2081-2095 (1989). https://doi.org:10.1084/jem.170.6.2081

4 Acuner Ozbabacan, S. E., Gursoy, A., Nussinov, R. & Keskin, O. The structural pathway of interleukin 1 (IL-1) initiated signaling reveals mechanisms of oncogenic mutations and SNPs in inflammation and cancer. *PLoS Comput Biol* **10**, e1003470 (2014). https://doi.org:10.1371/journal.pcbi.1003470

5 Freeman, G. J. *et al.* Engagement of the PD-1 immunoinhibitory receptor by a novel B7 family member leads to negative regulation of lymphocyte activation. *J Exp Med* **192**, 1027-1034 (2000).

6 Rodrigues Mantuano, N., Natoli, M., Zippelius, A. & Laubli, H. Tumor-associated carbohydrates and immunomodulatory lectins as targets for cancer immunotherapy. *J Immunother Cancer* **8** (2020). https://doi.org:10.1136/jitc-2020-001222

7 Laubli, H. & Varki, A. Sialic acid-binding immunoglobulin-like lectins (Siglecs) detect self-associated molecular patterns to regulate immune responses. *Cell Mol Life Sci* **77**, 593-605 (2020). https://doi.org:10.1007/s00018-019-03288-x

8 Pinho, S. S. & Reis, C. A. Glycosylation in cancer: mechanisms and clinical implications. *Nat Rev Cancer* **15**, 540-555 (2015). https://doi.org:10.1038/nrc3982

9 Marino, K. V., Cagnoni, A. J., Croci, D. O. & Rabinovich, G. A. Targeting galectin-driven regulatory circuits in cancer and fibrosis. *Nat Rev Drug Discov* **22**, 295-316 (2023). https://doi.org:10.1038/s41573-023-00636-2

10 Cagnoni, A. J. *et al.* Galectin-1 fosters an immunosuppressive microenvironment in colorectal cancer by reprogramming CD8(+) regulatory T cells. *Proc Natl Acad Sci U S A* **118** (2021). https://doi.org:10.1073/pnas.2102950118

11 Paschall, A. V. M., D. R.; Avci, F. Y. in *Encyclopedia of Cell Biology, Second Edition* (ed R. A.; Hart Bradshaw, G. W.; Stahl, P. D.) 404-413 (Elsevier, 2023).

12 Beatson, R. *et al.* The mucin MUC1 modulates the tumor immunological microenvironment through engagement of the lectin Siglec-9. *Nat Immunol* **17**, 1273-1281 (2016). https://doi.org:10.1038/ni.3552

13 Marcos, N. T. *et al.* Role of the human ST6GalNAc-I and ST6GalNAc-II in the synthesis of the cancer-associated sialyl-Tn antigen. *Cancer Res* **64**, 7050-7057 (2004). https://doi.org:10.1158/0008-5472.CAN-04-1921

14 Schultz, M. J. *et al.* The Tumor-Associated Glycosyltransferase ST6Gal-I Regulates Stem Cell Transcription Factors and Confers a Cancer Stem Cell Phenotype. *Cancer Res* **76**, 3978-3988 (2016). https://doi.org:10.1158/0008-5472.CAN-15-2834

372 15 Freire, T., Lo-Man, R., Bay, S. & Leclerc, C. Tn glycosylation of the MUC6 protein modulates its
373 immunogenicity and promotes the induction of Th17-biased T cell responses. *J Biol Chem* **286**,
374 7797-7811 (2011). https://doi.org:10.1074/jbc.M110.209742
375 16 Saeland, E. *et al.* The C-type lectin MGL expressed by dendritic cells detects glycan changes on
376 MUC1 in colon carcinoma. *Cancer Immunol Immunother* **56**, 1225-1236 (2007).
377 https://doi.org:10.1007/s00262-006-0274-z
378 17 van Vliet, S. J., Gringhuis, S. I., Geijtenbeek, T. B. & van Kooyk, Y. Regulation of effector T cells by
379 antigen-presenting cells via interaction of the C-type lectin MGL with CD45. *Nat Immunol* **7**, 1200-
380 1208 (2006). https://doi.org:10.1038/ni1390
381 18 Cheever, M. A. *et al.* The prioritization of cancer antigens: a national cancer institute pilot project
382 for the acceleration of translational research. *Clin Cancer Res* **15**, 5323-5337 (2009).
383 https://doi.org:10.1158/1078-0432.CCR-09-0737
384 19 Tumoglu, B., Keelaghan, A. & Avci, F. Y. Tn antigen interactions of macrophage galactose-type
385 lectin (MGL) in immune function and disease. *Glycobiology* **33**, 879-887 (2023).
386 https://doi.org:10.1093/glycob/cwad083
387 20 Wang, Y. *et al.* Cosmc is an essential chaperone for correct protein O-glycosylation. *Proc Natl*
388 *Acad Sci U S A* **107**, 9228-9233 (2010). https://doi.org:10.1073/pnas.0914004107
389 21 Ju, T., Aryal, R. P., Kudelka, M. R., Wang, Y. & Cummings, R. D. The Cosmc connection to the Tn
390 antigen in cancer. *Cancer Biomark* **14**, 63-81 (2014). https://doi.org:10.3233/CBM-130375
391 22 Beatson, R. *et al.* The Breast Cancer-Associated Glycoforms of MUC1, MUC1-Tn and sialyl-Tn, Are
392 Expressed in COSMC Wild-Type Cells and Bind the C-Type Lectin MGL. *PLoS One* **10**, e0125994
393 (2015). https://doi.org:10.1371/journal.pone.0125994
394 23 Beatson, R. E., Taylor-Papadimitriou, J. & Burchell, J. M. MUC1 immunotherapy. *Immunotherapy*
395 **2**, 305-327 (2010). https://doi.org:10.2217/imt.10.17
396 24 Siroy, A. *et al.* MUC1 is expressed at high frequency in early-stage basal-like triple-negative breast
397 cancer. *Hum Pathol* **44**, 2159-2166 (2013). https://doi.org:10.1016/j.humpath.2013.04.010
398 25 Burchell, J. M., Beatson, R., Graham, R., Taylor-Papadimitriou, J. & Tajadura-Ortega, V. O-linked
399 mucin-type glycosylation in breast cancer. *Biochem Soc Trans* **46**, 779-788 (2018).
400 https://doi.org:10.1042/BST20170483
401 26 Chen, D. *et al.* Immunotherapy of spontaneous mammary carcinoma with fusions of dendritic
402 cells and mucin 1-positive carcinoma cells. *Immunology* **109**, 300-307 (2003).
403 27 Mukherjee, P. *et al.* MUC1-specific immune therapy generates a strong anti-tumor response in a
404 MUC1-tolerant colon cancer model. *Vaccine* **25**, 1607-1618 (2007).
405 https://doi.org:10.1016/j.vaccine.2006.11.007
406 28 Lakshminarayanan, V. *et al.* Immune recognition of tumor-associated mucin MUC1 is achieved by
407 a fully synthetic aberrantly glycosylated MUC1 tripartite vaccine. *Proc Natl Acad Sci U S A* **109**,
408 261-266 (2012). https://doi.org:10.1073/pnas.1115166109
409 29 Loureiro, L. R. *et al.* Challenges in Antibody Development against Tn and Sialyl-Tn Antigens.
410 *Biomolecules* **5**, 1783-1809 (2015). https://doi.org:10.3390/biom5031783
411 30 Rodriguez, E. *et al.* Fasciola hepatica Immune Regulates CD11c+ Cells by Interacting with the
412 Macrophage Gal/GalNAc Lectin. *Front Immunol* **8**, 264 (2017).
413 https://doi.org:10.3389/fimmu.2017.00264
414 31 Singh, S. K. *et al.* Characterization of murine MGL1 and MGL2 C-type lectins: distinct glycan
415 specificities and tumor binding properties. *Mol Immunol* **46**, 1240-1249 (2009).
416 https://doi.org:10.1016/j.molimm.2008.11.021
417 32 Kumamoto, Y., Hirai, T., Wong, P. W., Kaplan, D. H. & Iwasaki, A. CD301b+ dendritic cells suppress
418 T follicular helper cells and antibody responses to protein antigens. *Elife* **5** (2016).
419 https://doi.org:10.7554/eLife.17979
420 33 Kumamoto, Y. *et al.* CD301b(+) dermal dendritic cells drive T helper 2 cell-mediated immunity.
421 *Immunity* **39**, 733-743 (2013). https://doi.org:10.1016/j.immuni.2013.08.029

422 34 Kenkel, J. A. *et al.* An Immunosuppressive Dendritic Cell Subset Accumulates at Secondary Sites
423 and Promotes Metastasis in Pancreatic Cancer. *Cancer Res* **77**, 4158-4170 (2017).
424 https://doi.org:10.1158/0008-5472.CAN-16-2212
425 35 da Costa, V. *et al.* The Tn antigen promotes lung tumor growth by fostering immunosuppression
426 and angiogenesis via interaction with Macrophage Galactose-type lectin 2 (MGL2). *Cancer Lett*
427 **518**, 72-81 (2021). https://doi.org:10.1016/j.canlet.2021.06.012
428 36 Ju, T. & Cummings, R. D. A unique molecular chaperone Cosmc required for activity of the
429 mammalian core 1 beta 3-galactosyltransferase. *Proc Natl Acad Sci U S A* **99**, 16613-16618 (2002).
430 https://doi.org:10.1073/pnas.262438199
431 37 Matsumoto, Y. *et al.* Identification of Tn antigen O-GalNAc-expressing glycoproteins in human
432 carcinomas using novel anti-Tn recombinant antibodies. *Glycobiology* **30**, 282-300 (2020).
433 https://doi.org:10.1093/glycob/cwz095
434 38 Breed, E. R. *et al.* Type 2 cytokines in the thymus activate Sirpalpha(+) dendritic cells to promote
435 clonal deletion. *Nat Immunol* **23**, 1042-1051 (2022). https://doi.org:10.1038/s41590-022-01218-x
436 39 Kumamoto, Y., Denda-Nagai, K., Aida, S., Higashi, N. & Irimura, T. MGL2 Dermal dendritic cells are
437 sufficient to initiate contact hypersensitivity in vivo. *PLoS One* **4**, e5619 (2009).
438 https://doi.org:10.1371/journal.pone.0005619
439 40 Izumi, G. *et al.* CD11b(+) lung dendritic cells at different stages of maturation induce Th17 or Th2
440 differentiation. *Nat Commun* **12**, 5029 (2021). https://doi.org:10.1038/s41467-021-25307-x
441 41 Bottcher, J. P. & Reis e Sousa, C. The Role of Type 1 Conventional Dendritic Cells in Cancer
442 Immunity. *Trends Cancer* **4**, 784-792 (2018). https://doi.org:10.1016/j.trecan.2018.09.001
443 42 Haniffa, M. *et al.* Human tissues contain CD141hi cross-presenting dendritic cells with functional
444 homology to mouse CD103+ nonlymphoid dendritic cells. *Immunity* **37**, 60-73 (2012).
445 https://doi.org:10.1016/j.immuni.2012.04.012
446 43 Liu, P., Zhao, L., Kroemer, G. & Kepp, O. Conventional type 1 dendritic cells (cDC1) in cancer
447 immunity. *Biol Direct* **18**, 71 (2023). https://doi.org:10.1186/s13062-023-00430-5
448 44 Saito, Y., Komori, S., Kotani, T., Murata, Y. & Matozaki, T. The Role of Type-2 Conventional
449 Dendritic Cells in the Regulation of Tumor Immunity. *Cancers (Basel)* **14** (2022).
450 https://doi.org:10.3390/cancers14081976
451 45 Pal, B. *et al.* A single-cell RNA expression atlas of normal, preneoplastic and tumorigenic states in
452 the human breast. *EMBO J* **40**, e107333 (2021). https://doi.org:10.15252/embj.2020107333
453 46 Mantovani, A. *et al.* The chemokine system in diverse forms of macrophage activation and
454 polarization. *Trends Immunol* **25**, 677-686 (2004). https://doi.org:10.1016/j.it.2004.09.015
455 47 Zhang, S. *et al.* C1q(+) tumor-associated macrophages contribute to immunosuppression through
456 fatty acid metabolic reprogramming in malignant pleural effusion. *J Immunother Cancer* **11**
457 (2023). https://doi.org:10.1136/jitc-2023-007441
458 48 Yang, J. *et al.* Integrated genomic and transcriptomic analysis reveals unique characteristics of
459 hepatic metastases and pro-metastatic role of complement C1q in pancreatic ductal
460 adenocarcinoma. *Genome Biol* **22**, 4 (2021). https://doi.org:10.1186/s13059-020-02222-w
461 49 Yang, Q. *et al.* Single-Cell RNA Sequencing Reveals the Heterogeneity of Tumor-Associated
462 Macrophage in Non-Small Cell Lung Cancer and Differences Between Sexes. *Front Immunol* **12**,
463 756722 (2021). https://doi.org:10.3389/fimmu.2021.756722
464 50 Chen, L. *et al.* NLRP3 in tumor-associated macrophages predicts a poor prognosis and promotes
465 tumor growth in head and neck squamous cell carcinoma. *Cancer Immunol Immunother* **72**,
466 1647-1660 (2023). https://doi.org:10.1007/s00262-022-03357-4
467 51 Daley, D. *et al.* NLRP3 signaling drives macrophage-induced adaptive immune suppression in
468 pancreatic carcinoma. *J Exp Med* **214**, 1711-1724 (2017). https://doi.org:10.1084/jem.20161707
469 52 Li, F. L. *et al.* INHBA promotes tumor growth and induces resistance to PD-L1 blockade by
470 suppressing IFN-gamma signaling. *Acta Pharmacol Sin* **46**, 448-461 (2025).
471 https://doi.org:10.1038/s41401-024-01381-x
472 53 Mantovani, A., Allavena, P., Sica, A. & Balkwill, F. Cancer-related inflammation. *Nature* **454**, 436-
473 444 (2008). https://doi.org:10.1038/nature07205

54 Grivennikov, S. I., Greten, F. R. & Karin, M. Immunity, inflammation, and cancer. *Cell* **140**, 883-899 (2010). https://doi.org:10.1016/j.cell.2010.01.025

55 Liu, T., Zhang, L., Joo, D. & Sun, S. C. NF-kappaB signaling in inflammation. *Signal Transduct Target Ther* **2**, 17023- (2017). https://doi.org:10.1038/sigtrans.2017.23

56 Qian, Y., Kang, Z., Liu, C. & Li, X. IL-17 signaling in host defense and inflammatory diseases. *Cell Mol Immunol* **7**, 328-333 (2010). https://doi.org:10.1038/cmi.2010.27

57 Medzhitov, R. Origin and physiological roles of inflammation. *Nature* **454**, 428-435 (2008). https://doi.org:10.1038/nature07201

58 Harris, N. L. E. *et al.* SerpinB2 regulates stromal remodelling and local invasion in pancreatic cancer. *Oncogene* **36**, 4288-4298 (2017). https://doi.org:10.1038/onc.2017.63

59 Shuman Moss, L. A., Jensen-Taubman, S. & Stetler-Stevenson, W. G. Matrix metalloproteinases: changing roles in tumor progression and metastasis. *Am J Pathol* **181**, 1895-1899 (2012). https://doi.org:10.1016/j.ajpath.2012.08.044

60 Yang, Y. *et al.* The Apelin/APLNR system modulates tumor immune response by reshaping the tumor microenvironment. *Gene* **834**, 146564 (2022). https://doi.org:10.1016/j.gene.2022.146564

61 Ehira, N. *et al.* An embryo-specific expressing TGF-beta family protein, growth-differentiation factor 3 (GDF3), augments progression of B16 melanoma. *J Exp Clin Cancer Res* **29**, 135 (2010). https://doi.org:10.1186/1756-9966-29-135

62 Burdick, M. D., Harris, A., Reid, C. J., Iwamura, T. & Hollingsworth, M. A. Oligosaccharides expressed on MUC1 produced by pancreatic and colon tumor cell lines. *J Biol Chem* **272**, 24198-24202 (1997).

63 Hofmann, B. T. *et al.* COSMC knockdown mediated aberrant O-glycosylation promotes oncogenic properties in pancreatic cancer. *Mol Cancer* **14**, 109 (2015). https://doi.org:10.1186/s12943-015-0386-1

64 Madsen, C. B. *et al.* Glycan elongation beyond the mucin associated Tn antigen protects tumor cells from immune-mediated killing. *PLoS One* **8**, e72413 (2013). https://doi.org:10.1371/journal.pone.0072413

65 Medzhitov, R. The spectrum of inflammatory responses. *Science* **374**, 1070-1075 (2021). https://doi.org:10.1126/science.abi5200

66 Bruni, D., Angell, H. K. & Galon, J. The immune contexture and Immunoscore in cancer prognosis and therapeutic efficacy. *Nat Rev Cancer* **20**, 662-680 (2020). https://doi.org:10.1038/s41568-020-0285-7

67 Thorsson, V. *et al.* The Immune Landscape of Cancer. *Immunity* **48**, 812-830 e814 (2018). https://doi.org:10.1016/j.immuni.2018.03.023

68 van der Meijs, N. L., Travecedo, M. A., Marcelo, F. & van Vliet, S. J. The pleiotropic CLEC10A: implications for harnessing this receptor in the tumor microenvironment. *Expert Opin Ther Targets* **28**, 601-612 (2024). https://doi.org:10.1080/14728222.2024.2374743

69 Geijtenbeek, T. B. & Gringhuis, S. I. C-type lectin receptors in the control of T helper cell differentiation. *Nat Rev Immunol* **16**, 433-448 (2016). https://doi.org:10.1038/nri.2016.55

70 Biswas, S. K. & Mantovani, A. Macrophage plasticity and interaction with lymphocyte subsets: cancer as a paradigm. *Nat Immunol* **11**, 889-896 (2010). https://doi.org:10.1038/ni.1937

71 Mills, C. D., Lenz, L. L. & Harris, R. A. A Breakthrough: Macrophage-Directed Cancer Immunotherapy. *Cancer Res* **76**, 513-516 (2016). https://doi.org:10.1158/0008-5472.CAN-15-1737

72 Leone, R. D. & Powell, J. D. Metabolism of immune cells in cancer. *Nat Rev Cancer* **20**, 516-531 (2020). https://doi.org:10.1038/s41568-020-0273-y

73 Macauley, M. S., Crocker, P. R. & Paulson, J. C. Siglec-mediated regulation of immune cell function in disease. *Nat Rev Immunol* **14**, 653-666 (2014). https://doi.org:10.1038/nri3737

74 Andrews, S. FastQC: A Quality Control Tool for High Throughput Sequence Data. Available online at: http://www.bioinformatics.babraham.ac.uk/projects/fastqc. (2010).

75 Kim, D., Paggi, J. M., Park, C., Bennett, C. & Salzberg, S. L. Graph-based genome alignment and genotyping with HISAT2 and HISAT-genotype. *Nat Biotechnol* **37**, 907-915 (2019). https://doi.org:10.1038/s41587-019-0201-4

76 Liao, Y., Smyth, G. K. & Shi, W. featureCounts: an efficient general purpose program for assigning sequence reads to genomic features. *Bioinformatics* **30**, 923-930 (2014). https://doi.org:10.1093/bioinformatics/btt656

77 Love, M. I., Huber, W. & Anders, S. Moderated estimation of fold change and dispersion for RNA-seq data with DESeq2. *Genome Biol* **15**, 550 (2014). https://doi.org:10.1186/s13059-014-0550-8

78 Xu, S. *et al.* Using clusterProfiler to characterize multiomics data. *Nat Protoc* **19**, 3292-3320 (2024). https://doi.org:10.1038/s41596-024-01020-z

79 Edgar, R., Domrachev, M. & Lash, A. E. Gene Expression Omnibus: NCBI gene expression and hybridization array data repository. *Nucleic Acids Res* **30**, 207-210 (2002). https://doi.org:10.1093/nar/30.1.207

80 Hao, Y. *et al.* Dictionary learning for integrative, multimodal and scalable single-cell analysis. *Nat Biotechnol* **42**, 293-304 (2024). https://doi.org:10.1038/s41587-023-01767-y

81 McGinnis, C. S., Murrow, L. M. & Gartner, Z. J. DoubletFinder: Doublet Detection in Single-Cell RNA Sequencing Data Using Artificial Nearest Neighbors. *Cell Syst* **8**, 329-337 e324 (2019). https://doi.org:10.1016/j.cels.2019.03.003

82 Nofech-Mozes, I., Soave, D., Awadalla, P. & Abelson, S. Pan-cancer classification of single cells in the tumour microenvironment. *Nat Commun* **14**, 1615 (2023). https://doi.org:10.1038/s41467-023-37353-8

83 Hu, C. *et al.* CellMarker 2.0: an updated database of manually curated cell markers in human/mouse and web tools based on scRNA-seq data. *Nucleic Acids Res* **51**, D870-D876 (2023). https://doi.org:10.1093/nar/gkac947

84 Cheng, S. *et al.* A pan-cancer single-cell transcriptional atlas of tumor infiltrating myeloid cells. *Cell* **184**, 792-809 e723 (2021). https://doi.org:10.1016/j.cell.2021.01.010

Figure legends:

Fig. 1. CD301b/Tn Axis Impacts Tumor Growth

A. AT3 (Tn^{low}) and AT3 *Cosmc* KO cells (Tn^{hi}) (2.5E5/mouse) were injected into the mammary pads of C57BL/6 mice (n = 25). Tumor sizes were monitored. Tumor sizes were calculated based on (length times $width^2$)/2 for volumes in mm^3. **B.** AT3 (Tn^{low}) and AT3 *Cosmc* KO cells (Tn^{hi}) tumor cells ($2.5x10^5$/mouse) were injected into the mammary pads of WT mice and heterozygous Mgl2-DTR mice (n= 4 or 5) with or without $CD301b^+$ cells depleted. Tumor sizes were monitored. **C.** AT3 *Cosmc* KO cells (Tn^{hi}) ($2.5x10^5$/mouse) were injected into the mammary pads of *Mgl2* KO mice (n=5). Tumor sizes were monitored.

Fig. 2. Characterization of $CD45^+CD301b^+$ immune cells in murine breast cancer TME.

562 Single cell suspensions from tumors of WT mice injected with AT3 *Cosmc* KO cells (Tn^{hi}) were
563 stained, and expressions of surface markers were analyzed with flow cytometry (gated as in Suppl.
564 Fig. 2). **A.** Among live $CD45^+$ cells, $CD301b^+$ cells are $CD11c^+$. **B.** $CD301b^+$ and $CD11c^+$ cells are
565 $MHCII^+$ and $CD11b^+$. **C.** $CD301b^+$ and $CD11c^+$ cells are cDC2. DCs and cDC2s in the TME, **D**
566 **and E**, respectively, consist of Cd301b-negative and positive cells.

567 **Fig. 3. Characterization of $CD45^+CD301b^+$ immune cells in human breast cancer TME.**

568 **A.** UMAP of all immune cells colored by major lineage (B/Plasma cell, Dendritic cell,
569 Macrophage/Monocyte, NK cell, T cell). **B.** Immune cells highlighting $CLEC10A^+$ cells (colored)
570 over all cells (gray). **C.** Bar plot showing the fraction of $CLEC10A^+$ cells within each major lineage.
571 **D.** UMAP of dendritic cell compartment colored by subset (cDC1, cDC2, cDC-$LAMP3^+$, pDC). **E.**
572 Dendritic cell subset highlighting $CLEC10A^+$ cells (colored) over all DCs (gray). **F.** Bar plot
573 showing the fraction of $CLEC10A^+$ cells within each DC subset. **G.** UMAP of macrophage
574 compartment colored by subset: $C1QC^+$ macrophages, $INHBA^+$ macrophages, and $NLRP3^+$
575 macrophages. **H.** Macrophage subset highlighting $CLEC10A^+$ cells (colored) over all macrophages
576 (gray). **I.** Bar plot showing the fraction of $CLEC10A^+$ cells within each macrophage subset.
577 *UMAP axes indicate the first two dimensions. Percentages in bar plots are calculated as*
578 *($CLEC10A^+$ cells / total cells) within the indicated group.*

579 **Fig. 4. The lack of CD301b is associated with a strong inflammatory immune signature in the**
580 **breast TME**

581 **A.** Heatmap showing differentially expressed genes (DEGs) identified by RNA-seq from tumors in
582 *Mgl2* KO and WT mice. The blue and red bands indicate low and high gene expression quantity,
583 respectively. Biological replicates showed the highest degree of correlation. **B.** Gene Set
584 Enrichment Analysis (GSEA) of Hallmark pathways reveals immune-related and cancer-associated
585 pathways, all of which are upregulated in Mgl2 KO. **C.** GSEA of KEGG pathways shows immune-
586 related and cancer-associated pathways, and they are all upregulated in Mgl2 KO. **D.** Volcano plot

587 showing the pathway-associated genes (from panels B and C). The genes with a $\log_2$ fold change
588 of 2 or greater are highlighted in purple. The X-axis represents $\log_2$-transformed fold change, and
589 the Y-axis represents $-\log_{10}$-transformed significance. The VENN diagram shows the distribution
590 of genes between Hallmark and KEGG gene sets. **E.** Volcano plot of DEGs between tumors from
591 *Mgl2* KO and WT mice. Red points indicate upregulated DEGs, blue points indicate downregulated
592 DEGs, gray points represent non-significant genes, and purple points indicate the pathway-
593 associated genes (from panel D). All the genes with a $\log_2$ fold change ≥ 2 are labeled.

594 **Supplementary Fig. 1.**

595 Generation of AT3 *Cosmc* KO (Tn^{hi}) murine breast cancer cells. **A. and B.** CRISPR-Cas9 KO of
596 Cosmc chaperone increases Tn cell surface expression in AT3 murine breast cancer cells. AT3
597 (Tn^{low}) and AT3 *Cosmc* KO (Tn^{hi}) cells were stained with **A.** mouse anti-Tn (reBaGs6 IgM) primary
598 and anti-IgM secondary antibodies, with secondary antibody-only as a control, and **B.** biotinylated
599 VVL followed by fluorescently-conjugated streptavidin, with fluorescently-conjugated
600 streptavidin-only as a control. **C.** RNA was isolated from AT3 (Tn^{low}) and AT3 *Cosmc* KO cells
601 (Tn^{hi}). qPCR was performed in triplicate wells using validated *Cosmc* qPCR primers and using b-
602 actin as a control for each sample. Fold changes were normalized against the average of AT3 *Cosmc*
603 KO cells (Tn^{hi}). **D.** AT3 (Tn^{low}) and AT3 *Cosmc* KO cells (Tn^{hi}) were cultured in 96 well plates
604 (n=5) at 1E4 cells/200mL for 3 days at 37oC. MTT proliferation assay was performed to determine
605 cell growth.

606 **Supplementary Fig. 2.**

607 Flow cytometry gating strategy for identifying dendritic cells and their subsets. DCs were identified
608 by expressions of MHCII and CD11c (bottom, middle, right) among $CD45^+$ cells (top, right).
609 Isotype control of CD11c antibody was used to locate $CD11c^+$ cells (bottom, right). cDC1s and
610 cDC2s were identified by expressions of CD103 and SIRP-alpha (bottom, middle, left). Total
611 $CD45^+$ cells were used to locate $CD103^{-/+}$, and SIRP-$alpha^{-/+}$ cells (bottom, left).

612 **Supplementary Fig. 3.**

613 **A.** Heatmap showing canonical markers used to define major immune cell lineages (B/Plasma cell,
614 Dendritic cell, Macrophage/Monocyte, NK cell, and T cell). **B.** Bar plots showing the frequency of
615 CLEC10A$^+$ cells across major immune lineages in ER$^+$, HER2$^+$, and triple-negative (TN) breast
616 cancers. **C.** Heatmap displaying canonical dendritic cell subset markers used to define cDC1, cDC2,
617 cDC-LAMP3$^+$, and pDC populations. **D.** Corresponding bar plots showing CLEC10A$^+$ proportions
618 within each DC subset across ER$^+$, HER2$^+$, and TN tumors. **E.** Heatmap showing markers used to
619 define macrophage polarization and functional states, including C1QC$^+$ macrophages, INHBA$^+$
620 macrophages, and NLRP3$^+$ macrophages. **F.** Bar plots showing the proportion of CLEC10A$^+$ cells
621 within each macrophage subtype across ER$^+$, HER2$^+$, and TN breast cancers.

622 *Heatmaps display scaled average expression per cell group. Bar plots represent the percentage of*
623 *CLEC10A$^+$ cells within each indicated population.*

624

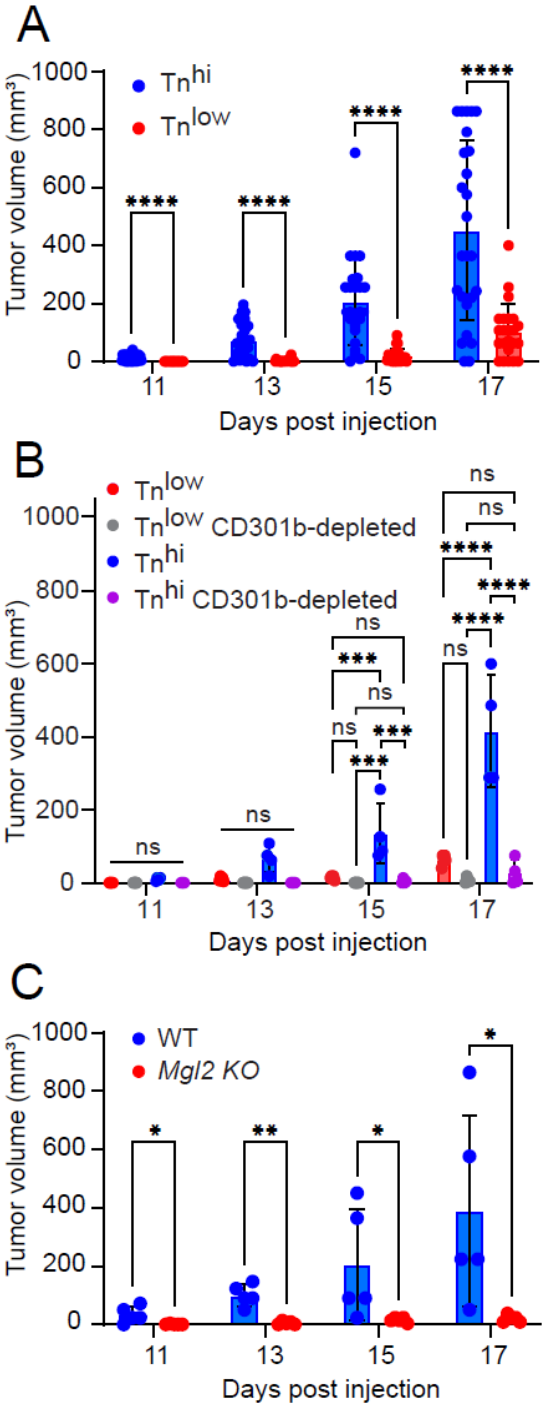
A
Tn^hi
Tn^low
Tumor volume (mm³)
1000
800
600
400
200
0
****
****
****
****
11
13
15
17
Days post injection
B
Tn^low
Tn^low CD301b-depleted
Tn^hi
Tn^hi CD301b-depleted
Tumor volume (mm³)
1000
800
600
400
200
0
ns
ns
ns
***
ns
ns
***
***
ns
ns
****
****
****
ns
11
13
15
17
Days post injection
C
WT
Mgl2 KO
Tumor volume (mm³)
1000
800
600
400
200
0
*
**
*
*
11
13
15
17
Days post injection

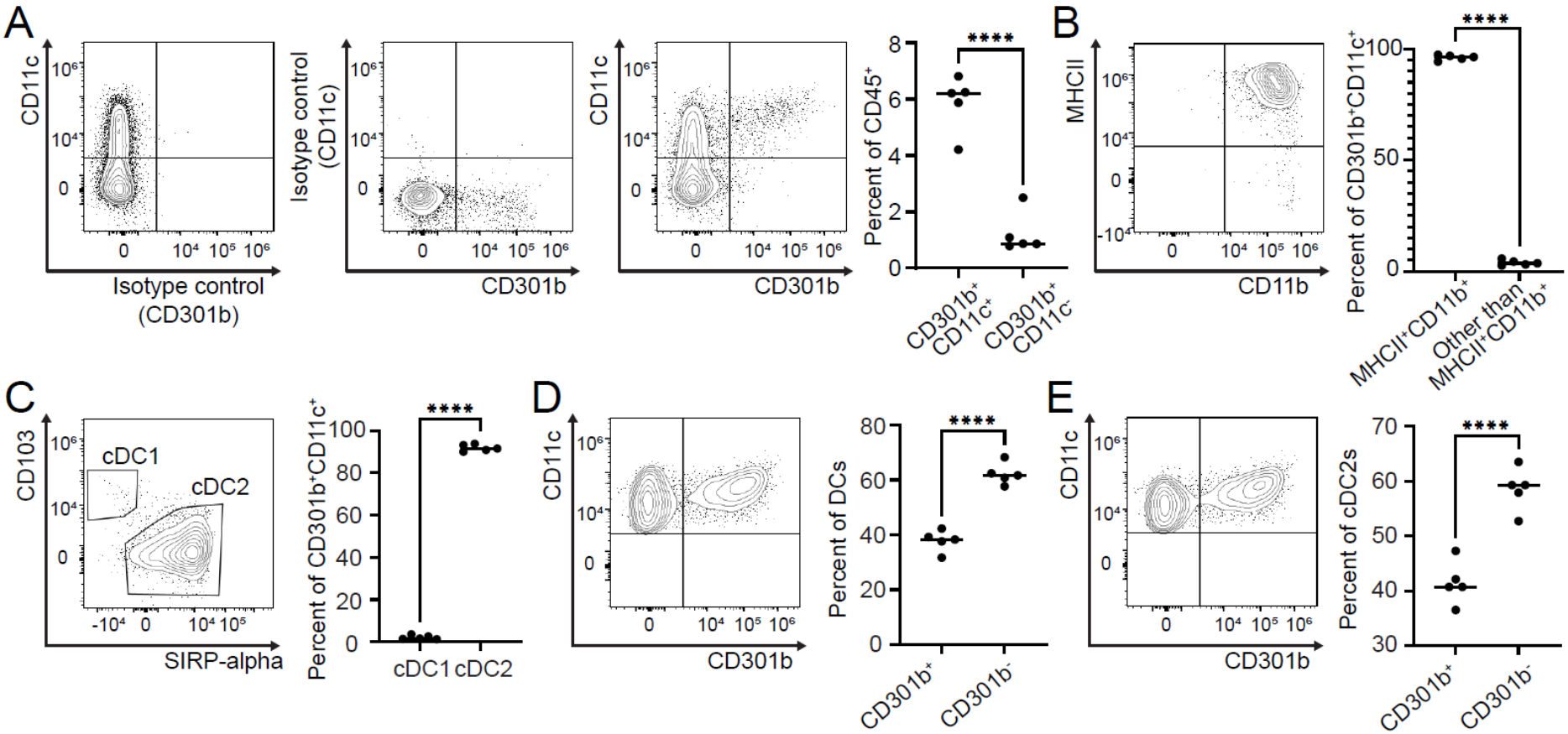
A
CD11c
Isotype control (CD301b)
Isotype control (CD11c)
CD301b
CD11c
CD301b
Percent of CD45+
****
CD301b+ CD11c+
CD301b+ CD11c-
B
MHCII
CD11b
Percent of CD301b+CD11c+
****
MHCII+CD11b+
Other than MHCII+CD11b+
C
CD103
cDC1
cDC2
SIRP-alpha
Percent of CD301b+CD11c+
****
cDC1
cDC2
D
CD11c
CD301b
Percent of DCs
****
CD301b+
CD301b-
E
CD11c
CD301b
Percent of cDC2s
****
CD301b+
CD301b-

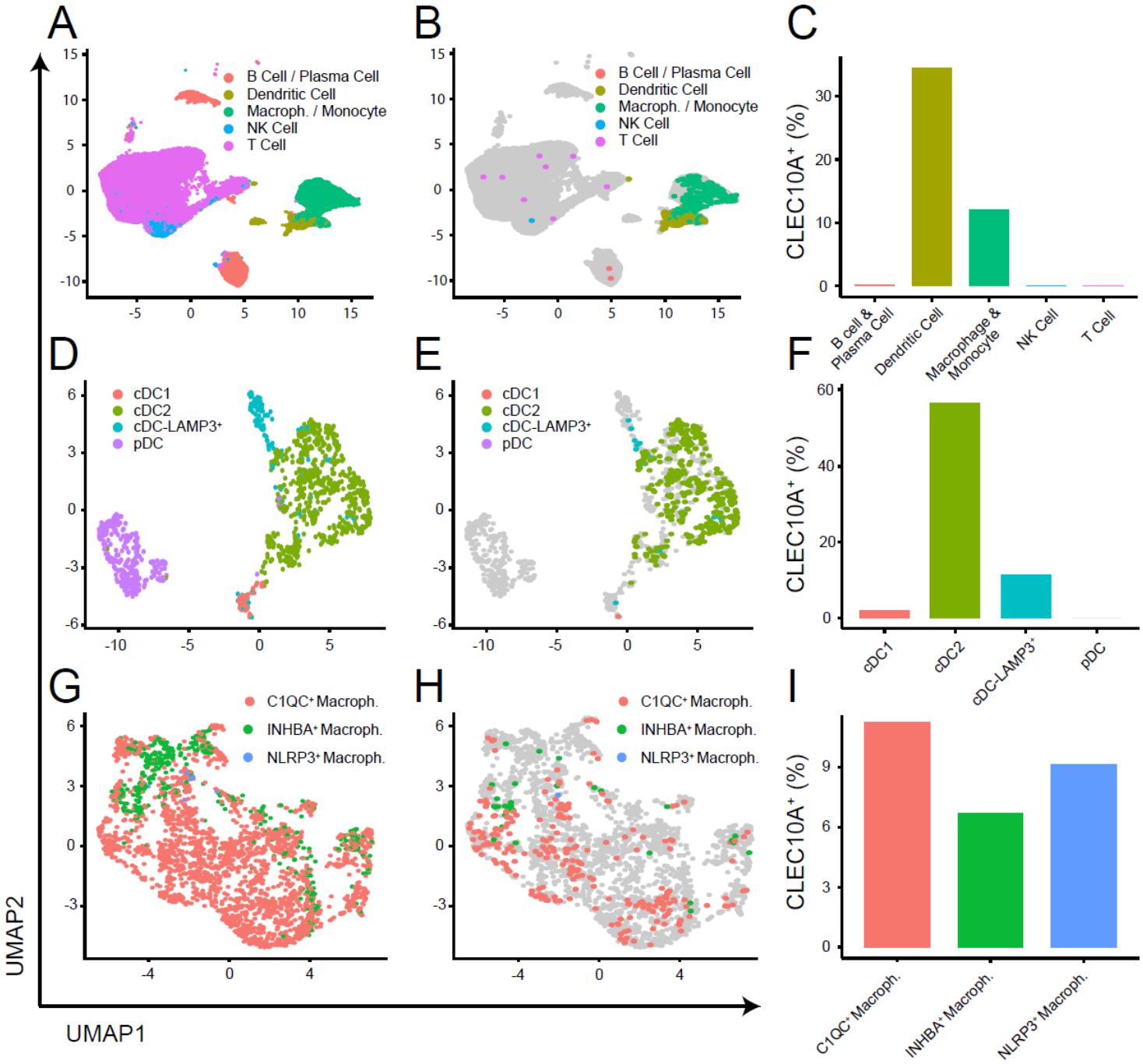
A
B Cell / Plasma Cell
Dendritic Cell
Macroph. / Monocyte
NK Cell
T Cell
B
B Cell / Plasma Cell
Dendritic Cell
Macroph. / Monocyte
NK Cell
T Cell
C
CLEC10A+ (%)
B cell & Plasma Cell
Dendritic Cell
Macrophage & Monocyte
NK Cell
T Cell
D
cDC1
cDC2
cDC-LAMP3+
pDC
E
cDC1
cDC2
cDC-LAMP3+
pDC
F
CLEC10A+ (%)
cDC1
cDC2
cDC-LAMP3+
pDC
G
C1QC+ Macroph.
INHBA+ Macroph.
NLRP3+ Macroph.
H
C1QC+ Macroph.
INHBA+ Macroph.
NLRP3+ Macroph.
I
CLEC10A+ (%)
C1QC+ Macroph.
INHBA+ Macroph.
NLRP3+ Macroph.
UMAP2
UMAP1

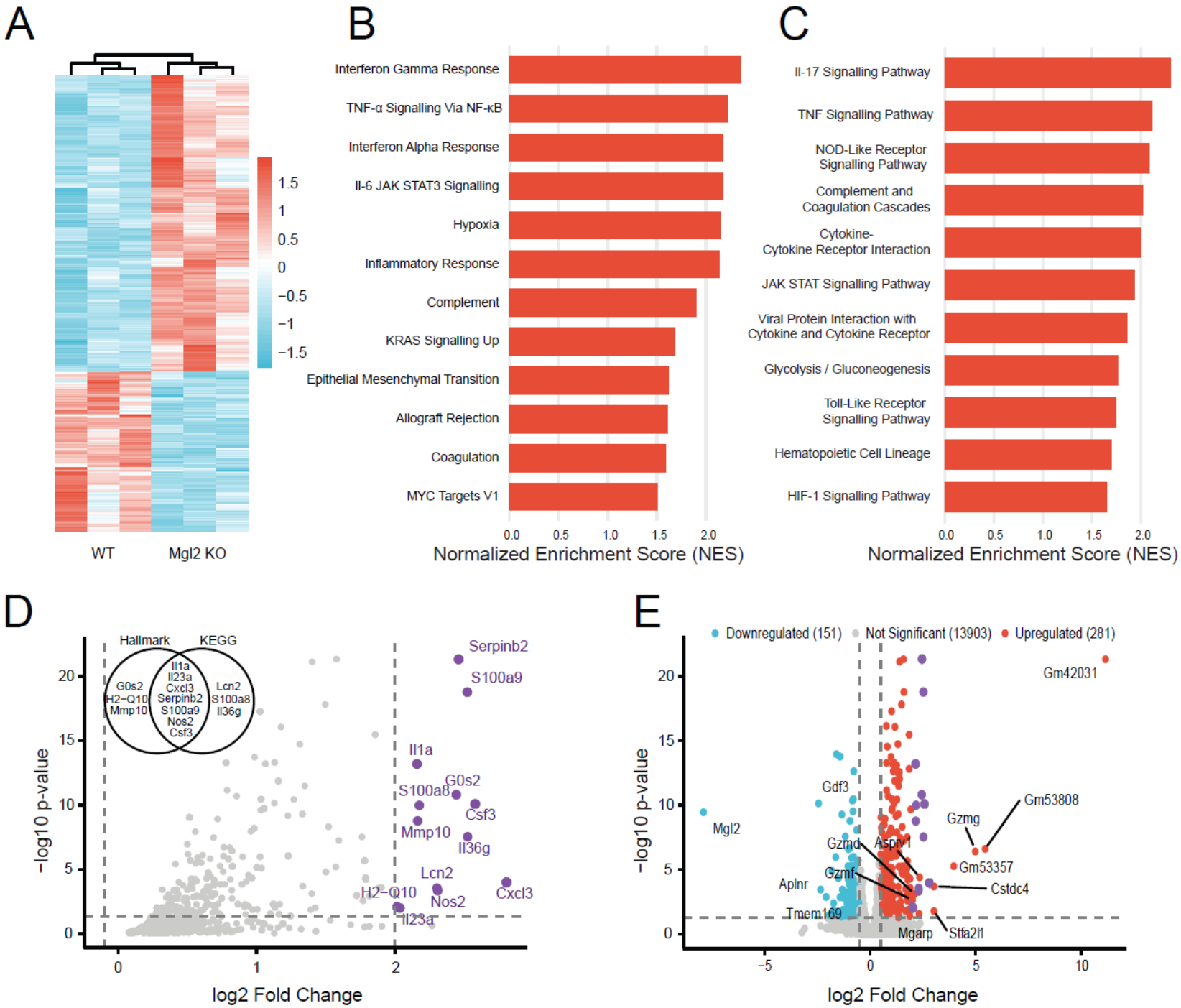
A
1.5
1
0.5
0
−0.5
−1
−1.5
WT
Mgl2 KO
B
Interferon Gamma Response
TNF-α Signalling Via NF-κB
Interferon Alpha Response
Il-6 JAK STAT3 Signalling
Hypoxia
Inflammatory Response
Complement
KRAS Signalling Up
Epithelial Mesenchymal Transition
Allograft Rejection
Coagulation
MYC Targets V1
0.0 0.5 1.0 1.5 2.0
Normalized Enrichment Score (NES)
C
Il-17 Signalling Pathway
TNF Signalling Pathway
NOD-Like Receptor Signalling Pathway
Complement and Coagulation Cascades
Cytokine-Cytokine Receptor Interaction
JAK STAT Signalling Pathway
Viral Protein Interaction with Cytokine and Cytokine Receptor
Glycolysis / Gluconeogenesis
Toll-Like Receptor Signalling Pathway
Hematopoietic Cell Lineage
HIF-1 Signalling Pathway
0.0 0.5 1.0 1.5 2.0
Normalized Enrichment Score (NES)
D
Hallmark
KEGG
G0s2
H2−Q10
Mmp10
Il1a
Il23a
Cxcl3
Serpinb2
S100a9
Nos2
Csf3
Lcn2
S100a8
Il36g
−log10 p-value
log2 Fold Change
Serpinb2
S100a9
Il1a
G0s2
S100a8
Csf3
Mmp10
Il36g
Lcn2
H2−Q10
Nos2
Cxcl3
Il23a
E
Downregulated (151)
Not Significant (13903)
Upregulated (281)
Gm42031
Gdf3
Mgl2
Gzmg
Gm53808
Gzmd
Aspn
Gm53357
Gzmf
Aplnr
Cstdc4
Tmem169
Mgarp
Stfa2l1
−log10 p-value
log2 Fold Change